

X-ray observation of ULAS J1120+0641, the most distant quasar at $z=7.08$

A. Moretti¹, L. Ballo¹, V. Braitto¹, A. Caccianiga¹, R. Della Ceca¹, R. Gilli², R. Salvaterra³, P. Severgnini¹, C. Vignali⁴

¹ INAF, Osservatorio Astronomico di Brera, Via Brera 28, 20121, Milano, Italy

² INAF, Osservatorio Astronomico di Bologna, Via Ranzani 1, 40127, Bologna, Italy

³ INAF, Via E. Bassini 15, 20133 Milano, Italy

⁴ Dipartimento di Astronomia, Università degli Studi di Bologna, Via Ranzani 1, 40127 Bologna, Italy

Received ; accepted

ABSTRACT

Aims. We aim at probing the emission mechanism of the accreting super massive black holes in the high redshift Universe.

Methods. We study the X-ray spectrum of ULAS1120+0641, the highest redshift quasar detected so far at $z=7.085$, which has been deeply observed (340 ks) by XMM-Newton.

Results. Despite the long integration time the spectral analysis is limited by the poor statistics, with only 150 source counts being detected. We measured the spectrum in the 2-80 keV rest-frame (0.3-10 keV observed) energy band. Assuming a simple power law model we find a photon index of 2.0 ± 0.3 and a luminosity of $6.7 \pm 0.3 \cdot 10^{44}$ erg s⁻¹ in the 2-10 keV band, while the intrinsic absorbing column can be only loosely constrained ($N_H < 10^{23}$ cm⁻²). Combining our measure with published data, we calculate that the X-ray-to-optical spectral index α_{OX} is 1.8 ± 0.1 , in agreement with the α_{OX} -UV luminosity correlation valid for lower redshift quasars.

Conclusions. We expanded to high energies the coverage of the spectral energy distribution of ULAS1120+0641. This is the second time that a $z > 6$ quasar has been investigated through a deep X-ray observation. In agreement with previous studies of $z \sim 6$ AGN samples, we do not find any hint of evolution in the broadband energy distribution. Indeed from our dataset ULAS 1120+0641 is indistinguishable from the population of optically bright quasar at lower redshift.

1. Introduction

High redshift AGNs are important probes of the Universe at the end of the Dark Ages, before or around the time when the first stars formed. Characterising their multi-wavelength properties allows us to investigate the formation and early evolution of the super massive black holes (SMBHs) and their interaction with the host galaxies.

In the last decade wide area optical-IR photometric surveys succeeded in finding a statistically significant number (~ 50) of AGNs at redshift $5.7 < z < 6.4$ (Fan et al. 2006; Jiang et al. 2009; Willott et al. 2010b). Complementing these data with IR spectroscopy for a subsample of 10 quasars, Willott et al. (2010a) derived the mass function at $z > 6$, which can be used to constrain models of SMBH evolution (Di Matteo et al. 2008; Marconi et al. 2008; Shankar et al. 2009; Volonteri 2010). Recently, Venemans et al. (2013) discovered three $z > 6.5$ quasars in the optical/IR VIKING 332 deg² survey, setting a lower limit of 1.1 Gpc^{-3} on the density of SMBH with mass larger than $10^9 M_\odot$ at $6.5 < z < 7.5$.

Few of these high redshift sources have been studied through their X-ray emission. Three have been observed for 10-30 ks by Chandra with 5-20 photons collected for each one (Shemmer et al. 2006). For the only SDSS J1030+0524 at $z=6.3$ a deep (100 ks) XMM-Newton observation has been carried out and a spectroscopic study has been reported (Farrah et al. 2004). The statistical X-ray properties of $5 < z < 6$ AGNs have been studied so far only by stacking samples of several sources (Vignali et al. 2005; Shemmer et al. 2006). Overall these stud-

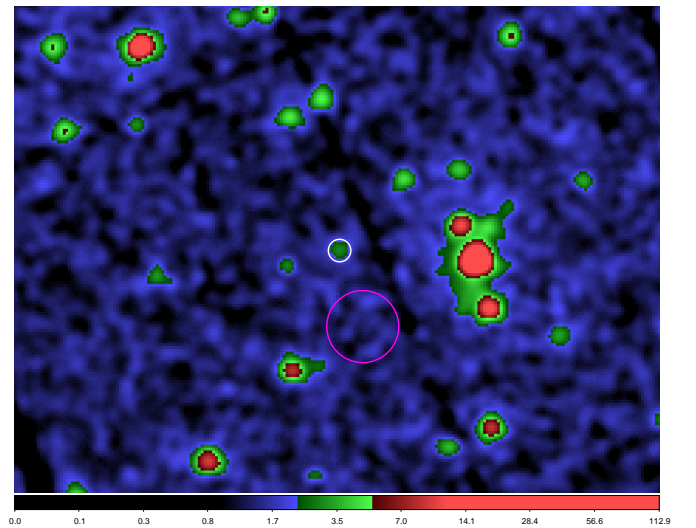


Fig. 1. The 4'' kernel smoothed XMM-Newton MOS image of ULAS1120+0641 region of the sky in the (observed) 0.5-2.0 keV band. The white and magenta circles show the source and background extraction regions of 10'' and 32'' radius, respectively.

ies indicated that the quasar broadband energy distribution has not significantly evolved over cosmic time, at least out to $z=6$. Indeed, the mean X-ray spectral slope at $z > 5$ is indistinguishable from the local population, while the ratio between UV and X-ray is consistent with the values observed at lower redshift.

Orbit	date	nom. exp.	eff. exp (MOS,PN)
2281	May 23 2012	111.0	75.98, 69.69
2294	Jun 18 2012	122.9	101.5, 86.95
2295	Jun 20 2012	97.67	83.27, 64.61

Table 1. XMM-Newton observation log. In the third column we report the nominal exposure times in ks, while in the last column we report the effective exposures (after data cleaning) used in the spectral analysis for both instruments. Effective exposures are identical for MOS1 and MOS2.

In this paper we discuss the deep XMM-Newton observation of ULAS J1120+0641, the highest redshift quasar detected so far ($z=7.085$). It has been discovered in the UK Infrared Deep Sky Survey (UKIDSS) and deeply studied by means of deep VLT and Gemini North spectroscopic observations (Mortlock et al. 2011). Starting from an absolute magnitude of $M_{1450,AB}=-26.6\pm0.1$ and using a correction of 4.4, Mortlock et al. (2011) estimated a bolometric luminosity of $2.4\times10^{47}\text{erg s}^{-1}$, while the mass of the accreting black hole has been measured to be $2.0^{+1.5}_{-0.7}\times10^9 M_\odot$ (Mortlock et al. 2011). This implies an Eddington ratio of $1.2^{+0.6}_{-0.5}$ (Mortlock et al. 2011). Very recently De Rosa et al. (2013) refined the estimate of the black hole mass and of the bolometric luminosity by means of a new VLT/X-Shooter deep observation. They measured a mass of $2.4^{+0.2}_{-0.2}\times10^9 M_\odot$ and an Eddington ratio of 0.5.

ULAS J1120+0641 has been also observed in the 1-2 GHz band by Momjian et al. (2014) who set an upper limit on the ratio of the observed radio to the optical flux densities of $R<0.5-4.3$ (depending on the assumed radio spectral index α). Therefore, irrespective of the assumed spectral index, the source J1120+0641 at $z = 7.085$ is a radio quiet quasar.

The very fact that a $2\times10^9 M_\odot$ black hole exists 750 million years after the Big Bang strongly constrains the mass of the seed from which it developed, which cannot be lower than $5\times10^5 M_\odot$, unless it grew by means of thousands of merging events with massive star remnants (Willott 2011). Exploiting the detection of the [CII] emission line from the host galaxy, Venemans et al. (2012) were able to estimate the star formation rate ($160-440 \odot \text{yr}^{-1}$), the dust mass ($0.7-6\times10^8 M_\odot$) and an upper limit on the dynamical mass of $(3.6\times10^{10}(\sin i)^{-2} M_\odot)$. While the spectrum red-ward of the Ly α is almost indistinguishable from lower redshift quasar, the blue-ward part brings to an estimate of the neutral fraction of the IGM of >0.1 , which is 15 times higher than $z \sim 6$ (Mortlock et al. 2011; Bolton et al. 2011).

While writing this paper, another work presenting the analysis of the same dataset, has been posted on arXiv (Page et al. 2013). We will discuss the differences between their analysis and ours throughout the paper.

Throughout this paper we assume $H_0=70 \text{ km s}^{-1}$ and $\Omega_\Lambda=0.73$ and $\Omega_m=0.27$.

2. Data

XMM-Newton observed ULAS1120+0641 in three different orbits in the period from May 24th to June 21st 2012 for a total of 340 ks (Tab. 1). The data are publicly available from the XMM science archive¹. EPIC data have been processed and cleaned using the Science Analysis Software (SAS ver 13.0.1) and analyzed using standard software packages (FTOOLS ver. 6.13). The data were filtered for high background time intervals; for

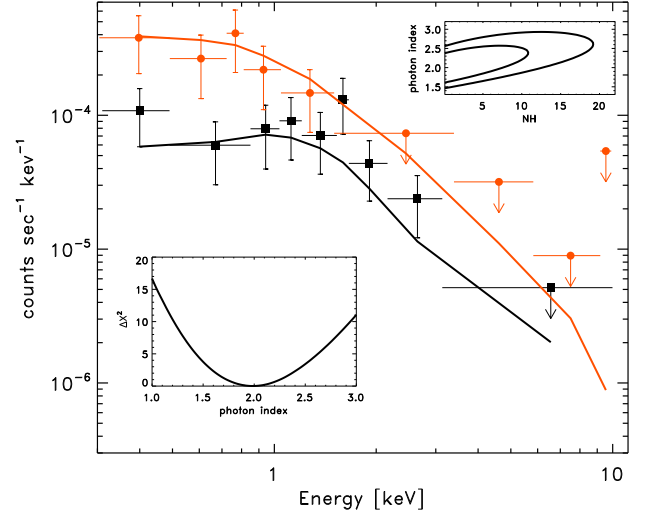


Fig. 2. Black and red points and lines show the MOS and PN data and models, with the relative 1σ errors. We detect significant emission up to ~ 3 keV. For the clarity of the plot, data are binned in order to have a 2σ significance in each bin. Arrows show the 2σ upper limits. In the lower inset the $\Delta\chi^2$ is shown for different values of photon index. In the upper inset the $\Delta\chi^2$ contour plot is shown as a function of the photon index and the N_H at the 68% and 90% confidence level (for 2 parameters of interest).

each observation and EPIC camera, we extracted the 10-12 keV light curves and filtered out the time intervals where the light curve was 2σ above the mean. For the scientific analysis we considered only events corresponding to patterns 0-12 and pattern 0-4 for the EPIC-MOS1/MOS2 and EPIC-pn, respectively. We ended up with 260.75 and 221.25 useful ks for the MOS and the PN, respectively (Tab. 1).

We restricted our spectral analysis to a circular region centred on the optical position of the source (RA: 11:20:01.48 DEC:06:41:24.3) with a radius of $10''$, corresponding to 55% of the encircled energy fraction at 1.5 keV². The background was extracted from an adjacent circular region, ~ 10 times larger (Fig.1). In the source region and in the 0.3-2.0 (0.3-10) keV observed energy band, the source is 45% and 30% (28% and 10%) of the total (source+background) signal, for the MOS and the PN respectively, while using a wider extraction region would result in an unacceptable signal/background ratio. We extracted the data from the same regions for both the MOS detectors and for the PN, summing together the six MOS and the three PN spectra respectively (together with the calibration matrices). In total the estimated source counts registered by the MOS and PN in the 0.3-10 keV band are ~ 86 and 71 , 95% of which are below 3.0 and 2.0 keV respectively, (Fig.2).

Using Xspec version 12.7.1 (Arnaud 1996), we modelled the MOS and PN spectra with a simple absorbed power law, the absorption factor being frozen to the Galactic value ($5.1\times10^{20} \text{ cm}^{-2}$) as measured by the HI Galaxy map (Kalberla et al. 2005). Spectra were grouped ensuring a minimum of one count for each bin and the best fit was calculated using the C-statistics. We found that the best photon index is $1.98^{+0.26}_{-0.26}$ (errors are quoted at 68% confidence level) and the flux in the 0.5-2.0 keV band is $9.3^{+1.3}_{-1.2}\times10^{-16} \text{ erg s}^{-1} \text{ cm}^{-2}$ (Tab.2).

¹ <http://xmm.esac.esa.int/xsa>; PI: M. Page

² http://xmm.esac.esa.int/external/xmm_user_support/documentation

N_H	5.1×10^{20}	(frozen)	cm^{-2}
norm.	4.16×10^{-7}	(3.65 - 4.70)	$\text{keV}^{-1} \text{s}^{-1} \text{cm}^{-2}$
ph.ind.	1.98	(1.72 - 2.26)	
Flux [0.5-2] keV	$9.3 \cdot 10^{-16}$	(8.2 - 10.6)	$\text{erg s}^{-1} \text{cm}^{-2}$
Lumin [2-10]keV	$6.7 \cdot 10^{44}$	(6.4 - 6.9)	erg s^{-1}
d.o.f.	637		
C-stat	693		

Table 2. Best fit parameters. The uncertainty intervals reported in the second column are at the 68% confidence level.

Folding the model with an absorber at the same redshift of the source (zwabs in XSPEC), the 1σ upper limit on the intrinsic absorbing column density is 10^{23} cm^{-2} . Although the redshifted iron K_α falls in a very favourable energy band (0.8 keV) both for detector energy resolution and response, we can set only a very loose 1σ upper limit of 0.92 keV (rest-frame) to its equivalent width.

Using the bolometric luminosity reported by Mortlock et al. (2011), $2.4 \times 10^{47} \text{ erg s}^{-1}$, yields $L_{\text{bol}}/L_{[2-10]\text{keV}}$ of 361^{+19}_{-15} , where the errors account only for the luminosity uncertainties.

Our spectral slope best fit is lower than the one reported by Page et al. (2013), who find $2.64^{+0.37}_{-0.33}$ (1σ errors). Although the two measures differ by less than 2σ , the discrepancy is more significant considering that the measure are not independent since we used the same dataset. A possible origin of this discrepancy is a different estimate of the background. It is well known that the X-ray background cosmic variance produces an extra systematic term to be summed to the poissonian/statistical uncertainty (Moretti et al. 2009). Moreover the instrument component, which is a substantial fraction of the EPIC background is not spatially uniform on the detector (Kuntz & Snowden 2008). To check our measure against its non-poissonian variations, we repeated our analysis varying five times the size and the position of the background extraction region: we found that the five photon indexes best fit values are in the range 1.6-2.3 with a mean of 1.9. Therefore we cannot exclude that a different background estimate is the cause of the difference between our spectroscopic measure with respect to the one reported by Page et al. (2013).

We note that our flux measure in the 0.5-2.0 keV band is 1.5 times ($\sim 2\sigma$) higher than the one reported by Page et al. (2013). As the background in the soft band is almost two times the source, this discrepancy can be explained by a 20-30% difference in the background normalization estimate. This, again, suggests that the probability that the difference between the 2 measures is due to a background fluctuation is not negligible.

ULAS1120+0641 has been observed by Chandra for 15.8 ks, in February 2011 (Observation-id 13203). We analysed the processed (level 2) event file available from the Chandra science archive³. Due to the short exposure only 4 source counts have been collected in the 0.5 -2.0 keV band. Assuming the spectral parameters measured by XMM-Newton, we would expect 2.8 counts in a 15.8 ks Chandra observation, consistent with the observed data. Thus, at variance with Page et al. (2013), we do not find a significant variation in the flux level of ULAS1120+0641, between the Chandra and XMM observations.

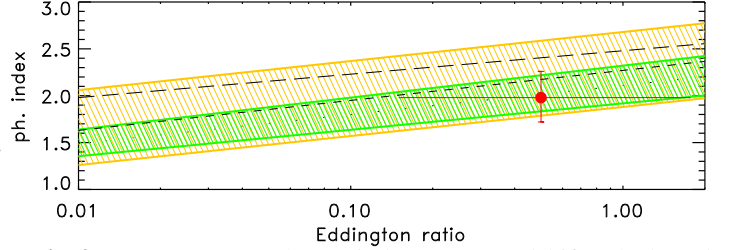
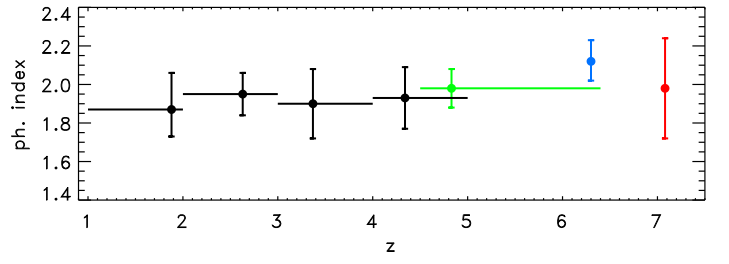


Fig. 3. Upper panel: photon index versus redshift. Black and green points are results of stacking analysis from Just et al. (2007) and Vignali et al. (2005); the blue point is the photon index of SDSS J1030+05 (Farrah et al. 2004); the red point is our measure of the photon index of ULASJ1120+0641. In all the cases the assumed model is a simple power law. Lower panel: photon index versus Eddington ratio. The yellow area represents the correlation together with its scatter found by Risaliti et al. (2009) while the green shaded area is from Shemmer et al. (2008). The short and long dashed line are from Brightman et al. (2013) and Fanali et al. (2013), respectively. Red point shows the present measure of the photon index of ULASJ1120+0641, with the Eddington ratio estimate by De Rosa et al. (2013). The error bar is calculated accounting for the zero point uncertainty (0.55 dex) of the relation used to compute the BH mass (De Rosa et al. 2013).

3. Discussion

3.1. X-ray photon index

According to the AGN standard model, X-ray photons are produced by the inverse Compton scattering of the accretion disk UV photons by the electrons in the corona (Haardt & Maraschi 1991). Therefore the X-ray spectrum can be used as a direct probe of the physical mechanisms acting very close to the black hole. In particular, the slope of the X-ray spectrum gives direct information about the energy distribution of the electrons in the corona. The typical AGN X-ray spectrum above 2 keV can be well described by a simple power law with a photon index of ~ 2 with a 10-20% dispersion either considering only data below 10 keV (Tozzi et al. 2006; Mainieri et al. 2007; Young et al. 2009; Corral et al. 2011, e.g.) or including higher energies (Burlon et al. 2011; Rivers et al. 2013, e.g.). As several previous studies (Vignali et al. 2005; Shemmer et al. 2006; Just et al. 2007) did not find any detectable evolution of the AGN photon index change with redshift up to $z \sim 5$, we expect that ULAS1120+0641 photon index would be consistent with the collective properties of lower redshift populations (upper panel of Fig.3). Indeed the measure of $1.98^{+0.26}_{-0.28}$ is well consistent with the typical 2.0 and a 10-20% scatter. The only other direct measure of a $z > 6$ AGN X-ray photon index is $\sim 2.1 \pm 0.1$ (Farrah et al. 2004), while the stacking analysis of a sample of 24 $z > 4.5$ quasars yields 1.98 ± 0.2 (Vignali et al. 2005).

³ <http://cda.harvard.edu/chaser/>

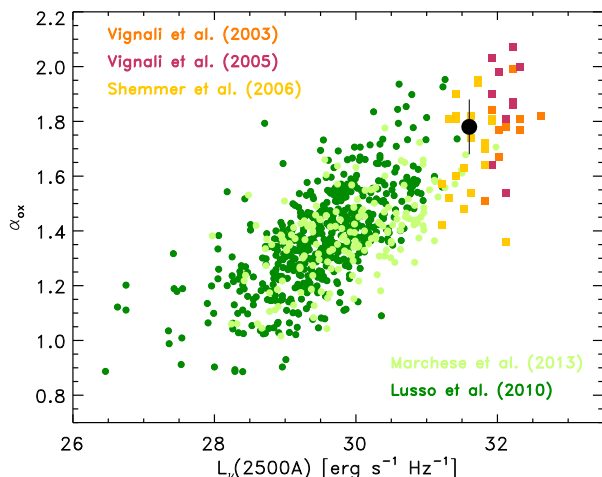


Fig. 4. The α_{OX} versus UV monochromatic luminosity of ULAS1120+0641 (black point), compared with four different samples, both X-ray (Lusso et al. 2010; Marchese et al. 2012) and optically selected (Vignali et al. 2003b, 2005; Shemmer et al. 2006)

A relation between the Eddington ratio and X-ray spectral slope has been found by several authors using different samples (Shemmer et al. 2006; Risaliti et al. 2009; Jin et al. 2012; Fanali et al. 2013; Brightman et al. 2013); see the lower panel of Fig. 3. A plausible physical interpretation of this correlation is that, at high accretion rates, the disk emission is stronger and produces more soft photons leading to a more efficient Compton cooling of the corona and, therefore, to steeper X-ray spectra. ULAS1120+0641, with an estimated Eddington ratio of 0.5 (De Rosa et al. 2013), according to Shemmer et al. (2008), Risaliti et al. (2009) and Fanali et al. (2013), is expected to have an X-ray spectrum slope of 2.0-2.4, which is within the 1σ uncertainty of the actual measure (lower panel of Fig. 3).

3.2. X-ray and UV

The ratio between X-ray and UV-optical emission is expected to be determined by the relative importance between disk and corona. Therefore it is an important piece of information to test energy generation models and to constrain the bolometric corrections. From a purely observational point of view, determining this ratio is mandatory to compare statistical properties of samples which have been selected at different wavelengths. The ratio between the UV and X-ray emission is usually parametrized by α_{OX} ⁴ which is the slope of the power law that joins the energy distribution at 2500Å and 2 keV.

For ULAS1120+06 we measured a 2 keV rest-frame monochromatic luminosity of $7.8^{+5.2}_{-3.1} \times 10^{26} \text{ erg s}^{-1} \text{ Hz}^{-1}$, while from the IR spectrum (Mortlock et al. 2011) we derived a 2500 Å rest-frame luminosity of $3.4 \times 10^{31} \text{ erg s}^{-1} \text{ Hz}^{-1}$, assuming a 10% uncertainty. This yields an $\alpha_{\text{OX}} = 1.78^{+0.10}_{-0.10}$.

Vignali et al. (2003a), Steffen et al. (2006) and, more recently, Lusso et al. (2010) found that the apparent dependence of α_{OX} on redshift can be explained by a selection bias, and confirmed that the real dependence is on the UV luminosity. Indeed all these authors found a significant correlation between α_{OX} and the monochromatic $L_{\nu}(2500\text{Å})$ in the sense that the X-

ray luminosity is relatively lower for UV brighter AGN (Fig. 4). In agreement with these results, we find that ULAS1120+06 α_{OX} is consistent with lower redshift ($4 < z < 5$) optically selected bright QSO I (Vignali et al. 2003b, 2005; Steffen et al. 2006; Just et al. 2007) which have similar UV luminosities. Moreover, we find very good consistency with the extrapolation to bright UV luminosities of the L_X - L_{UV} correlation as measured in the X-ray selected AGN COSMOS (Lusso et al. 2010) and XBS (Marchese et al. 2012) samples (Fig. 4).

Accordingly with what is found for the α_{OX} parameter, we note that the value of the X-ray bolometric correction, k_{bol} , defined as the ratio between the X-ray and bolometric luminosities (361^{+19}_{-15}), is well consistent with the expectation for quasars at this level of X-ray loudness (Lusso et al. 2010; Marchese et al. 2012). In particular, using the relation found by Marchese et al. (2012), $\log(k_{\text{bol}}) = 1.05 - 1.52\alpha_{\text{OX}} + 1.29\alpha_{\text{OX}}^2$ we expect a bolometric correction of 387 with a 1σ scatter of 54 (corresponding to 14%), which is in very good agreement with our measure.

4. Conclusion

In this paper we report on the deep X-ray observation of the quasar ULAS1120+0641. This is the second time that the X-ray spectrum, and, in particular, the direct measure of the photon index of an AGN at redshift $z > 6$ can be measured. We found that the X-rays contribute only for the 0.3% to the bolometric energy output of this source. Both the X-ray spectrum and the X-ray-to-optical spectral index are consistent with the properties of bright quasar samples optically detected at lower redshift. This suggests that the physical mechanism, which is behind the broadband emission of AGNs in the local Universe is already active in ULAS1120+064, only 0.75 Gyr after the Big Bang.

As pointed out by De Rosa et al. (2013), the systematic uncertainties in the mass determination (0.3-0.55 dex) prevent from placing robust constraints on the masses of the SMBH seeds. In this context the measure of the X-ray spectrum slope provides a useful extra piece of information since we know that this slope is related to the Eddington ratio. Our work shows that this is the case also for ULAS1120+064, for which the X-ray spectrum is consistent with the Eddington ratio independently determined from the optical spectrum.

In the last few years, wide area optical/IR photometric surveys have been able to extend the AGN studies at very high redshift well inside the re-ionisation era and when the coevolution with their host galaxies has been settling. This has been possible thanks to the detection of very bright and rare quasars, which represent the most striking sources of the AGN population, the bulk of which is much fainter. In this context X-ray observations would be mandatory to probe the obscured accretion. However, building an X-ray selected catalog of $z > 6$ AGNs is beyond the capabilities of the current generation of X-ray missions, which are limited by a relatively small grasp (effective area \times field of view). The wide field imager (WFI), which will be part of the scientific payload of the Athena+ mission (Nandra et al. 2013), recently selected as second large class mission (L2) in the Cosmic Vision program, will improve the survey velocity by two orders of magnitude with respect to Chandra. This will allow to detect a relevant number (60) of $z > 6$ AGN employing the same exposure time of the Chandra deep field, four millions seconds, (Aird et al. 2013).

At the present time, X-ray follow-up observations of optically/IR selected quasars are useful not only to calculate the bolometric luminosity and improve the accretion rates estimates,

⁴ defined as $\alpha_{\text{OX}} = -\log(f_{2500\text{Å}}/f_{2\text{keV}})/\log(\nu_{2500\text{Å}}/\nu_{2\text{keV}})$.

but also to test possible evolution of the physical mechanism acting very close to the SMBH. For high redshift AGNs this is very important as the measure of the mass, together with an estimate of the accretion rates for a statistically significant sample, can provide the constraints to distinguish between different models of SMBH formation and evolution (Volonteri 2010).

Acknowledgements. The research leading to these results has received funding from the European Commission Seventh Framework Programme (FP7/2007-2013) under grant agreement n.267251 "Astronomy Fellowships in Italy" (AstroFlt).

References

- Aird, J., Comastri, A., Brusa, M., et al. 2013, ArXiv e-prints
- Arnaud, K. A. 1996, in *Astronomical Society of the Pacific Conference Series*, Vol. 101, *Astronomical Data Analysis Software and Systems V*, ed. G. H. Jacoby & J. Barnes, 17
- Bolton, J. S., Haehnelt, M. G., Warren, S. J., et al. 2011, *MNRAS*, 416, L70
- Brightman, M., Silverman, J. D., Mainieri, V., et al. 2013, *MNRAS*, 433, 2485
- Burlon, D., Ajello, M., Greiner, J., et al. 2011, *ApJ*, 728, 58
- Corral, A., Della Ceca, R., Caccianiga, A., et al. 2011, *A&A*, 530, A42
- De Rosa, G., Venemans, B. P., Decarli, R., et al. 2013, ArXiv e-prints
- Di Matteo, T., Colberg, J., Springel, V., Hernquist, L., & Sijacki, D. 2008, *ApJ*, 676, 33
- Fan, X., Strauss, M. A., Becker, R. H., et al. 2006, *AJ*, 132, 117
- Fanali, R., Caccianiga, A., Severgnini, P., et al. 2013, *MNRAS*, 433, 648
- Farrar, D., Priddey, R., Wilman, R., Haehnelt, M., & McMahon, R. 2004, *ApJ*, 611, L13
- Haardt, F. & Maraschi, L. 1991, *ApJ*, 380, L51
- Jiang, L., Fan, X., Bian, F., et al. 2009, *AJ*, 138, 305
- Jin, C., Ward, M., & Done, C. 2012, *MNRAS*, 425, 907
- Just, D. W., Brandt, W. N., Shemmer, O., et al. 2007, *ApJ*, 665, 1004
- Kalberla, P. M. W., Burton, W. B., Hartmann, D., et al. 2005, *A&A*, 440, 775
- Kuntz, K. D. & Snowden, S. L. 2008, *A&A*, 478, 575
- Lusso, E., Comastri, A., Vignali, C., et al. 2010, *A&A*, 512, A34
- Mainieri, V., Hasinger, G., Cappelluti, N., et al. 2007, *ApJS*, 172, 368
- Marchese, E., Della Ceca, R., Caccianiga, A., et al. 2012, *A&A*, 539, A48
- Marconi, A., Axon, D. J., Maiolino, R., et al. 2008, *ApJ*, 678, 693
- Momjian, E., Carilli, C. L., Walter, F., & Venemans, B. 2014, *AJ*, 147, 6
- Moretti, A., Pagani, C., Cusumano, G., et al. 2009, *A&A*, 493, 501
- Mortlock, D. J., Warren, S. J., Venemans, B. P., et al. 2011, *Nature*, 474, 616
- Nandra, K., Barret, D., Barcons, X., et al. 2013, ArXiv e-prints
- Page, M. J., Simpson, C., Mortlock, D. J., et al. 2013, ArXiv e-prints
- Risaliti, G., Young, M., & Elvis, M. 2009, *ApJ*, 700, L6
- Rivers, E., Markowitz, A., & Rothschild, R. 2013, *ApJ*, 772, 114
- Shankar, F., Weinberg, D. H., & Miralda-Escudé, J. 2009, *ApJ*, 690, 20
- Shemmer, O., Brandt, W. N., Netzer, H., Maiolino, R., & Kaspi, S. 2008, *ApJ*, 682, 81
- Shemmer, O., Brandt, W. N., Schneider, D. P., et al. 2006, *ApJ*, 644, 86
- Steffen, A. T., Strateva, I., Brandt, W. N., et al. 2006, *AJ*, 131, 2826
- Tozzi, P., Gilli, R., Mainieri, V., et al. 2006, *A&A*, 451, 457
- Venemans, B. P., Findlay, J. R., Sutherland, W. J., et al. 2013, *ApJ*, 779, 24
- Venemans, B. P., McMahon, R. G., Walter, F., et al. 2012, *ApJ*, 751, L25
- Vignali, C., Brandt, W. N., & Schneider, D. P. 2003a, *AJ*, 125, 433
- Vignali, C., Brandt, W. N., Schneider, D. P., Garmire, G. P., & Kaspi, S. 2003b, *AJ*, 125, 418
- Vignali, C., Brandt, W. N., Schneider, D. P., & Kaspi, S. 2005, *AJ*, 129, 2519
- Volonteri, M. 2010, *A&A Rev.*, 18, 279
- Willott, C. 2011, *Nature*, 474, 583
- Willott, C. J., Albert, L., Arzoumanian, D., et al. 2010a, *AJ*, 140, 546
- Willott, C. J., Delorme, P., Reylé, C., et al. 2010b, *AJ*, 139, 906
- Young, M., Elvis, M., & Risaliti, G. 2009, *ApJS*, 183, 17